EXPLORING THE SENSITIVITY OF PRECIPITATION BEHAVIOR USING A SINGLE-COLUMN MODEL

BY

Kathryn Clark

Submitted to the graduate degree program in Geography and the Graduate Faculty of the University of Kansas in partial fulfillment of the requirements for the degree of Master of Science in Atmospheric Science

David B. Mechem
Chairperson

Nathaniel A. Brunsell

Dan Hirmas

Date Defended: March, 27, 2013

The Thesis Committee for Kathryn Clark
certifies that this is the approved version of the following thesis:

EXPLORING THE SENSITIVITY OF PRECIPITATION BEHAVIOR

USING A SINGLE-COLUMN MODEL

David B. Mechem
Chairperson

Nathaniel A. Brunsell

Dan Hirmas

Date Approved: March 27, 2013

ABSTRACT

Relationships between land-surface conditions, boundary layer (PBL) growth, atmospheric stability, and convective precipitation behavior are explored using the Weather Research and Forecasting Model (ARW WRF) in single column model (SCM) mode. SCMs are computationally inexpensive, which enables the exploration of a wide range of parameter space. This study aims to determine the effects of land properties and atmospheric stability on convective precipitation behavior, specifically addressing precipitation event frequency and magnitude, and bridge the gap between computationally expensive three-dimensional models and low-order bulk models. This study focuses on the effects of soil moisture and large-scale synoptic forcing on surface fluxes, PBL structure and evolution, and precipitation behavior for different vegetation fractions. Soil moisture conditions become less influential on precipitation behavior with increasing vegetation cover, and large-scale vertical motion becomes more important with increasing subsidence as events become more intense but less frequent. Changes to the low-level inversion weakly affects event frequency while free-tropospheric stability substantially influences total precipitation. Thermodynamic mixing diagrams capture the multi-day dynamics and preferential regions of thermodynamic parameter space where sharp boundaries are delineated. Results indicate that idealized SCMs are able to capture some aspects of land-atmosphere interactions (PBL response to soil moisture, precipitation event magnitude) but not others (precipitation frequency), suggesting the simplifying assumptions pertaining to synoptic forcing may not be justified in all cases.

ACKNOWLEDGMENTS

We wish to thank Josh Hacker for advice with the SCM version of WRF. This research was supported by the National Science Foundation (NSF) Experimental Program to Simulate Competitive Research (EPSCoR) grants, NSF EPS- 0553722, EPS-09194443, KAN0061396 and KAN0066263, and the U.S. Department of Energy (DOE) grant DE-SC0005359.

Table of Contents

List of Figures

List of Tables

Chapter 1

Introduction

Land-atmosphere interactions, specifically the relationship between land-surface conditions, planetary boundary layer (PBL) growth and development, and deep convective precipitation, are important aspects of regional climate (Clark and Arritt, 1995; Findell and Eltahir, 2003; Jones and Brunsell, 2009a,b; Santanello et al., 2007). Understanding precipitation behavior — total precipitation, event frequency and magnitude — is especially vital in rain fed agricultural regions because of the strong influence of precipitation behavior on vegetation status and crop productivity (Porporato et al., 2003). Precipitation event frequency and magnitude are especially important since they partially determine soil infiltration of rainfall available for vegetation or cause local runoff or flooding (Trenberth et al., 2003). The partitioning between precipitation event frequency and magnitude has been difficult to capture in numerical simulations (Dai, 2006), but this partitioning is important especially when considering agriculture health in a changing climate (Trenberth et al., 2003). Many general circulation models (GCMs) produce precipitation events that occur too frequently and at a reduced intensity (Dai and Trenberth, 2004; Sun et al., 2006) producing reasonable precipitation totals, but with incorrect frequency and magnitude of events. Errors in precipitation magnitude and frequency have strong implications for vegetation. Petrie and Brunsell (2012) found event frequency has a greater control

on soil moisture than event magnitude, but changes in event frequency and magnitude can strongly influence available soil moisture. Knapp et al. (2002) found that ecosystem responses to event intensity and frequency are significant and independent of changes in total precipitation as changes in rainfall variability strongly affects soil water content which influences plant water stress and productivity.

The interaction between soil moisture, PBL, and deep convective processes can be thought of in an idealized, 1D conceptual framework. Soil type, moisture, and vegetation characteristics strongly influence the partitioning of surface fluxes of mass and energy (Betts, 2000; Eagleson, 1978; McPherson, 2007; Seneviratne et al., 2010; Trier et al., 2004). Surface fluxes of heat and moisture govern the PBL budgets in the mixed layer and provide energy for deep convection, which produces precipitation and the accompanying drying and warming of the atmospheric column.

An understanding of the physical processes involved in land-atmosphere interactions is complicated by many non-linear responses (Brunsell, 2006; Findell and Eltahir, 2003). Land surface conditions (i.e. soil moisture state, θ, and vegetation fraction, VF) strongly influence PBL growth and potential for deep convection, ultimately determining the likelihood and magnitude of precipitation (Pielke, 2001; Segal et al., 1995; Trier et al., 2004). At the most basic level, soil moisture conditions and vegetation cover affect latent and sensible heat fluxes which act to moisten and heat the PBL, modifying its thermodynamic properties (Entekhabi et al., 1996; Stensrud, 2007). Vegetation cover proves to have a strong impact on the exchanges of energy between the surface and atmosphere (Betts, 2000; Clark and Arritt, 1995; McPherson, 2007; Seneviratne et al., 2010). These studies indicate that vegetation alter energy balance paritioning via the change of albedo and an effect on evapotranspiration through an increase in latent heat flux, with the later being the most influential (Betts, 2000; McPherson, 2007; Seneviratne et al., 2010) .

Moist static energy ($MSE = c_pT + gz + l_vq$), a thermodynamic state variable closely related to equivalent potential temperature (θ_e), has been used to discern whether precipitation will occur (Betts et al., 1994, 1996; De Ridder, 1997; Eltahir, 1998; Hohenegger et al., 2009; Santanello et al., 2011) as latent and sensible heat fluxes throughout the day can increase or decrease MSE. A decrease in Bowen ratio (H/LE, where H is sensible heat flux and LE is latent heat flux) from greater soil moisture results in reduced dry air entrainment into the PBL, a larger afternoon maximum of mixed-layer MSE, and ultimately greater potential for precipitation (Betts et al., 1996; De Ridder, 1997). Pal and Eltahir (2001) found with a shallower PBL, greater values of MSE resulted in increased frequency and magnitude of precipitation events. On the other hand, the increase in sensible heat flux associated with a larger Bowen ratio led to a greater entrainment of dry (low MSE) air into the PBL. Enhanced entrainment leads to a drier and warmer PBL state in the afternoon, reducing the potential for convective precipitation (Hohenegger et al., 2009).

Land-atmosphere interactions require an understanding of the coupling between surface fluxes, PBL growth, and convective precipitation. Some studies suggest that convective precipitation is not reliant on simply the amount of evapotranspiration resulting from wet or dry soil conditions, but more broadly the impact that the soil conditions and vegetation have on atmospheric stability and convective precipitation inititation (Seneviratne et al., 2010). It is becoming recognized that convective precipitation is dependent upon a wide range of land-surface and atmospheric controls above and beyond soil moisture (Juang et al., 2007a,b; Siqueira et al., 2009). We seek to characterize the sensitivity to multi-day convective precipitation behavior to differences in soil moisture, large-scale vertical motion (w_{ls}), vegetation fraction, large-scale advection, and atmospheric stability. The huge array of simulations implied by this wide number of factors suggests that full three-dimensional regional climate simula-

tions are not a practical modeling approach. For this reason, we employ an idealized single-column model (SCM) numerical framework. This technique features low computational expense and a theoretical framework consistent with our 1D conceptual framework of how the land surface, PBL, and deep convection interact. This study will examine how precipitation event magnitude and frequency vary with soil moisture and vegetation fraction. Finally, comparisons between the SCM model and observations will be made to assess the model's capability to portray precipitation behavior in the Great Plains.

Chapter 2

Methodology

This study is revolved around three-month summertime simulations for Topeka, Kansas (39.07°N, -95.62°W) using the Advanced Regional version of the Weather Research and Forecasting Model (ARW WRF) version 3.1 (Skamarock et al., 2005) run in SCM configuration.. Summer months are chosen because the majority of annual precipitation occurs between April and September in Topeka, KS. SCMs represent land-atmosphere interactions, PBL dynamics, and convective processes in a linked manner that is appropriate for studying soil moisture-convection feedback mechanisms (Siqueira et al., 2009). SCMs are also computationally inexpensive, which is ideal for exploring a wide range of parameter space.

Despite their computational attractiveness and relative simplicity, SCMs also possess some deficiencies addressing the relationship between soil moisture and convective precipitation. Guichard et al. (2004) found that the results from SCMs were consistent with those from 2D cloud-resolving models (CRMs), but the onset of precipitation in the SCM models was sooner than expected for the mid-latitude summertime convection. Additional disadvantages of the SCM framework include negligible synoptic and mesoscale advection, which can substantially influence convective development (Clark and Arritt, 1995; Koster and Eagleson, 1990; Segal et al., 1995). Furthermore, mesoscale organization associated with deep convection cannot be represented by the

lack of horizontal dimension in the SCM framework.

2.1 Model Description

The WRF-SCM model employs 23 vertical levels using a stretched vertical grid from the surface to 17 km at the model top with finer grid spacing (50 m - 650 m) within the PBL and 1 km grid spacing above 6 km. The Betts-Miller-Janjic (BMJ) convective parameterization scheme (Janjic, 1994) is employed in all simulations. Convection is triggered in this scheme if there is at least some convective available potential energy (CAPE), the cloud depth exceeds a critical height (cloud depth>200 hPa), and the atmosphere is relatively moist. This scheme works by adjusting the atmospheric sounding toward a post-convective reference profile derived from climatology. It is limited in the fact that it does not explicitly account for cap strength in inhibiting convection. WRF–SCM employs the boundary-layer parameterization of Yonsei University (YSU) scheme (Hong et al., 2006). Vertical convective transport is exclusively accomplished by the boundary-layer and deep convective parameterizations.

All simulations employ the 5-category ice-phase microphysical parameterization of Lin et al. (1983) which includes cloud water and cloud ice (non-precipitating categories), and rain, snow, and graupel (precipitating categories). Longwave radiation is parameterized using the Rapid Radiative Transfer Model (RRTM; Mlawer et al., 1997). Shortwave radiation is represented by the Dudhia parameterization (Dudhia, 1989), which includes clouds and clear-sky absorption and scattering.

The WRF-SCM simulations utilize the Noah land surface model (LSM; Chen and Dudhia, 2001; Ek et al., 2003). The Noah LSM has 4 soil layers. The first is a 10-cm top soil layer; the next layer is a 30-cm shallow root layer; the third layer is a 60-cm root zone; and the deep layer is a 100-cm sub-root zone. The Noah LSM incorporates direct soil and open water evaporation, canopy water evaporation, transpiration from

vegetation, and surface runoff amongst other processes.

2.2 Configuration of simulations

We conduct a suite of three-month simulations based on a representative July atmospheric profile and surface conditions (Table 1) for Topeka, Kansas (39.07°N, -95.62°W) and shortwave radiative forcing corresponding to perpetual July 1^{st} conditions (Schlemmer et al., 2012). Topeka, Kansas is chosen because of the well-documented, strong land-atmosphere coupling in the central Great Plains of North America (Koster et al., 2006). Figure 1 shows the initial sounding used for all simulations. The sounding is broadly representative of July conditions in northeast Kansas. The sounding shows a relatively moist boundary layer and lower troposphere, with atmospheric moisture decreasing substantially above approximately 500 mb. The sounding is characteristic of sunrise conditions — near-saturation conditions at the surface, overlaid by a stable layer and an elevated mixed layer. The sounding contains a substantial amount of instability (CAPE = 924.66 J kg^{-1}), with a small amount of convective inhibition (CIN) below 850 mb (CIN = –5.1 J kg^{-1}).

The atmospheric temperature is nudged to the original sounding over an adjustable timescale (1-7 days) in order to reach a representative temperature equilibrium (Schlemmer et al., 2012). The temperature nudging timescale (τ_n) can be thought of as a proxy for synoptic-scale advective forcing. We found that the model was well behaved without this forcing but converged to a radiative-convective equilibrium solution that was too warm. Atmospheric moisture is not nudged, however, acknowledging that atmospheric sources and sinks of moisture are in approximate balance as LE and precipitation are near moisture equilibrium. Simulations were performed with atmospheric moisture nudging, but the results were predictable and produced a large increase in precipitation event frequency.

Deep convection dries the column, warms the free troposphere, and cools the boundary layer. Deep convective overturning necessitates a period of "recovery" time to build up instability for the subsequent convective event. In our simulations, this destabilization results from a combination of H and LE, and the cooling of the free troposphere arising from nudging the temperature profile back to the initial state.

Initial soil temperatures (T_s) for all simulations are based on Atmospheric Radiation Measurement Program (ARM) measurements from site E6 in Towanda, Kansas (37.80°N, -96.99°W), the site closest to Topeka, Kansas. Measurements were taken from the beginning of July 2010. Soil moisture conditions are initialized from known soil moisture characteristics for silt loam soil texture (Rawls et al., 1982). Soil moisture is held constant throughout each simulation period in order to focus on precipitation event frequency and magnitude, and the effects of surface fluxes on PBL recovery time and evolution throughout each simulation. Holding soil moisture constant prohibits evaluation of feedbacks between soil moisture and precipitation. Trier et al. (2008) compared simulations with both constant soil moisture and interactive soil moisture over the U.S. Great Plains for a 12-day warm-season period. Results demonstrated that soil moisture evolution has little effect on mean thermodynamic variables and precipitation over this short of a time period. However, because this study is much longer (3-months), we are unable to evaluate soil moisture–precipitation feedbacks as seasonal changes in soil moisture can occur.

We explore some of the factors hypothesized to have a first-order effect on the behavior of deep-convective precipitation, given a specified thermodynamic profile: soil moisture, large-scale vertical motion (either subsidence or ascent), vegetation fraction, atmospheric stability, and nudging timescale. We employ the factor separation approach of Stein and Alpert (1993) and Dearden (2009) in order to evaluate the mutual interactions between factors, although we do not conduct every single simulation

in the parameter space shown in Table 1.

Simulations within the θ–w_{ls} parameter space will determine the effects that these variables have on the development and behavior of precipitation events. Various vegetation fractions (0, 0.5, 1 VF) are implemented to consider the impact on convective precipitation as vegetation cover affects surface energy balance, can decrease CIN through added moisture, and ultimately affect precipitation patterns over a given region (Brunsell, 2006; Juang et al., 2007b; McPherson, 2007). Large-scale vertical motion varies with passages of synoptic systems and mesoscale disturbances and can either promote or suppress convective precipitation through modulating atmospheric stability. Large-scale vertical motion is forced at every time step, and is valid at 2.5 km and "bowstrings" to zero at the surface and 5 km.

The soil moisture values range from wilting point to field capacity for silt loam soil texture (Rawls et al., 1982), and the vegetation used for all simulations is Noah LSM mixed dryland/irrigated cropland and pasture (Chen and Dudhia, 2001; Ek et al., 2003), which is indicative of the vegetation observed near Topeka, Kansas. The control run for this project is taken as vegetation fraction (VF)=1, θ=0.18 m^3 m^{-3}, and w_{ls}=0 cm s^{-1}, with a nudging timescale of 3 days. Three-month simulations provide a sufficient number of convective precipitation events (statistical realizations) to enable us to assess intermittency and convective precipitation behavior.

Chapter 3

Results

3.1 Control simulation

We performed a series of simulations to evaluate precipitation event frequency and magnitude, and its effects on PBL characteristics throughout the range of parameter space summarized in Table 1, but results from the control run simulation will be discussed first. Figure 2 shows the temporal evolution of variables from the control simulation representative of the middle part of the θ–w_{ls} parameter space (i.e. VF=1, θ=0.18 cm^3 cm^{-3}, and w$_{ls}$=0 cm s^{-1}). Time-height sections of mixing ratio (q (kg kg^{-1}); Fig. 2a) show that the simulation exhibits a regular oscillation of q increasing at low levels ($<$ 2 km) over the course of several days, followed by rapid reduction in low-level q and an increase in q in the free troposphere at heights ranging from the PBL depth up to $\sim$10 km. The abrupt changes in q are associated with convective precipitation events (Fig. 2d) and correspond to convection reducing the PBL moisture, and the detrainment of condensate moistening the free troposphere. Warming of the free troposphere from latent heat release (Fig. 2b) accompanies deep convective events. These results from the 90-day simulation compare favorably with the same simulation configuration run out to 5 years (not shown).

Figure 2d shows a number of precipitation events over the 90-day simulation period. Precipitation behavior is highly variable and exhibits single-day and multi-day

events of varying magnitudes (largest daily precipitation event=58.9 mm). Precipitation events are associated with large CAPE and low CIN. MSE typically increases leading up to a convective event, after which it decreases substantially. Often, an increase in MSE is not accompanied by an increase in CAPE, the reason being the stabilization of the free troposphere from prior convective events. CAPE increases when a combination of increasing surface MSE and cooling of the free troposphere (from the nudging term) results in buoyant convection for surface-based parcels. CIN is reduced (i.e., becomes closer to zero) leading up to a precipitation event, consistent with it acting as a "valve" for deep convective activity.

These figures show that MSE is not well correlated with deep convection occurrence. This is because MSE is a state variable relevant at the surface rather than a column property for a surface-based parcel. CAPE, on the other hand, is influenced by surface (or mixed-layer) MSE, but also free-tropospheric stability and the strength of the inversion at the top of the boundary layer.

The maximum daily PBL height varies but remains relatively low in the atmosphere (2-3 km) due to lower sensible heat flux, higher latent heat flux, and less entrainment of dry free tropospheric air. Stronger and more frequent precipitation events lead to lower PBL heights due to cooling in the lower levels from changes in energy partitioning between latent and sensible heat flux. This ultimately is what is responsible for the lower PBL heights, and is seen in both Fig. 2a and b.

The control run simulation produced precipitation that is highly variable in magnitude (daily precipitation magnitude ranges from 0.4 mm–58.9mm) and intermittency (days between events ranges from consecutive daily events–7 days) (Fig. 2d). The next section explores the sensitivity of precipitation across a wide range of the soil moisture and large-scale forcing parameter space.

3.2 Sensitivity simulation suites

The presence of vegetation promotes higher precipitation totals (Figs. 3a–c). For soil moisture less than ∼0.25 m^3 m^{-3}, total precipitation in the bare soil simulations (Fig. 3a) is predominantly controlled by the soil moisture (denoted by the dominate horizontal contours). For greater values of soil moisture, stronger precipitation is accompanied by higher values of large-scale vertical motion (i.e., larger w_{ls}). Perhaps unsurprisingly, precipitation is maximized for greatest values of soil moisture and large-scale ascent.

The suite of simulations with 50% vegetation fraction exhibits greater precipitation and some subtle differences with the bare soil simulation (Fig. 3b). Total precipitation varies predominantly as a function of soil moisture up to approximately 0.15 m^3 m^{-3}, above which large-scale vertical motion becomes important. In general, w_{ls} exerts greater importance in the 50% simulations than in the bare soil simulations.

Total precipitation for 100% vegetation (Fig. 3c) is strongly dependent upon vertical motion for values of w_{ls} less than about –0.1 cm s^{-1}. Above this value, strong precipitation was produced for soil moisture values above 0.12 m^3 m^{-3}. Note that in this idealized framework, large precipitation totals can be produced even in regimes of weak subsidence; strong upward vertical motion is not necessary to force deep convection. Once soil moisture reaches the threshold of ∼0.12 m^3 m^{-3}, it does not strongly influence total precipitation.

In summary, total precipitation is maximized under large-scale vertical ascent. This may come as no surprise as upward vertical motion is associated with precipitation while subsidence is associated with fair weather conditions. Vegetation fraction influences the the impact of soil moisture on precipitation, with increasing vegetation cover reducing the influence of soil moisture on convective precipitation, but

enhancing the influence of w_{ls}.

Figures 3d-f show the frequency of precipitation events (day^{-1}) for 0, 50, and 100% vegetation cover as a measure of precipitation intermittency. Low values of soil moisture in bare soil results in a large number of days between convective events, regardless of the large-scale vertical motion (Fig. 3d). For bare soil, precipitation events become more frequent with increasing soil moisture (Fig. 3d) but exhibit some dependence on vertical motion when θ>0.25 m^3m^{-3}. The dependence of event frequency on soil moisture is similar to the dependence of total precipitation, except the greatest influence of soil moisture on total precipitation occurs for intermediate values of soil moisture, whereas the greatest influence on event frequency occurs for smaller values of soil moisture. Increasing vegetation fraction increases precipitation frequency (Figs. 3d–f) and the dependence on large-scale vertical motion. Greater vegetation also isolates the influence of soil moisture to small values of soil moisture.

Although we do not formally address statistical significance, the cases of high precipitation intermittency (i.e., very small frequency of events) have very little statistical significance because over the 3-month simulation period, there are only 3-6 precipitation events.

Not surprisingly, precipitation event magnitude is greatly influenced by soil moisture in bare soil cases (Fig. 3g). The precipitation event magnitude for bare soil cases is generally low throughout the parameter space, but is largest in the subsidence regime. Event magnitude increases in the 50% and 100% coverage simulations throughout the parameter space, again peaking with subsidence (Fig. 3h–i). Intense precipitation events occur only when vegetation is present (Fig. 3h–i) and event magnitude exhibits a greater dependence on vertical motion rather than soil moisture, except for very low values of soil moisture. This behavior result reflects the relative magnitudes of transpiration vs. bare soil evaporation (mean LE flux for VF=1 is 140%

larger than VF=0) given available soil moisture. When vegetation is present, event magnitude is dependent more on vertical motion and less on soil moisture (Fig. 3h–i).

Low event magnitudes are likely associated with strong upward vertical motion because of the destabilizing effects of ascent trigger precipitation before substantial instability can form. On the other hand, simulations with strong subsidence exhibit stronger but less frequent events because the subsidence acts as a stabilizing influence until substantial instability can build to overcome it. Figure 3 shows that the greater frequency of smaller precipitation events under large-scale ascent ultimately produces more total precipitation than the low frequency, stronger events occurring under strong subsidence. This result is particularly robust for the vegetation-covered landscapes.

3.3 Comparison with observations

Figure 4 compares probability density functions (PDFs) of total precipitation, event frequency, and event magnitude estimated from the three simulation suites (VF=0, VF=0.5, VF=1) with corresponding observations. The observations were taken from the United States Historical Climatology Network in Lawrence, KS from 1900-2011 (Meene et al., 2011). To compare an observational record to the perpetual 1 July 90-day simulations, we used data from June–August. The PDFs in Fig. 4 are fit to gamma distributions (Furrer and Katz, 2008; Husak et al., 2006).

The PDFs for event magnitude for the simulations overlap substantially with the observational PDF (Fig. 4c), although the simulations slightly overestimate the mode and do not capture the right tail (extremes) of the distribution. The simulations produce a much smaller mode of precipitation event frequency than the observations (observation event frequency is ∼385% larger than simulations), and also overestimate the width of the distribution (observations range from ∼0.21–0.52 day^{-1} while

simulations range from ∼0–0.9 day^{-1}; Fig. 4b). The narrow distribution of event frequency from the observations is largely due to somewhat consistent frequency behavior year to year. These broad distributions translate into total precipitation PDFs that underestimate the mode (observational total precipitation ∼60% larger than VF=1 simulations, ∼108% larger than VF=0.5, and ∼370% larger than VF=0) and overestimate the width relative to the observational PDF (observations range from ∼105–660 mm while simulations range from ∼0–1100 mm; Fig. 4a). Two sample t-tests of the gamma distribution PDFs revealed no significant difference between observational data and model output for event magnitude, frequency, and total precipitation.

Figure 5 shows the shape (α) and scale (β) parameters for the gamma distribution of precipitation event magnitude and how they vary for all vegetation simulations. Observational values of α and β are overlaid. Blank sections indicate areas of the parameter space that have too few events and produce artificially inflated values of α (shape parameter) (Husak et al., 2006). Simulations with larger shape (α) values indicate situations with consistent day-to-day precipitation values. Areas of the parameter space with larger scale (β) parameter values are associated with a wider range in rainfall amounts (higher variance compared to the mean). The scale and shape parameters from the observational data overlay nicely onto the model output data, further indicating there is similar behavior of precipitation event magnitude between the model output and observational data from Lawrence, KS.

Event magnitudes from the simulations overlap the observational PDF. We interpret this as the model performing credibly with respect to the observations, especially in light of the highly idealized nature of the simulations. PDFs of event frequency and total precipitation, on the other hand, vary substantially between the observations and model.

3.4 PBL properties for full vegetation cases

Here we discuss PBL properties (LE, H, 2-m MSE, q_v, and θ) throughout the parameter space for VF=1 (100% vegetation simulations). The 3-month simulation daytime average LE flux for 100% vegetation cover (Fig. 6a) shows expected results. LE flux increases with increasing soil moisture. For a given amount of net radiation, larger latent heat flux means more water vapor in the boundary layer, less dry air entrainment from free tropospheric air, and greater surface-based MSE (Betts et al., 1996). This result may explain the good agreement between daytime average LE flux (Fig. 6a) and total precipitation (Fig. 3c).

Sensible heat flux (H) varies little over the parameter space, except for low soil moisture conditions ($\theta < 0.13$ m^{3}m^{-3}), where H becomes large. For these dry soils, total precipitation (Fig. 3c) is affected predominately by soil moisture. At higher soil moisture conditions, however, the relationship between surface fluxes and total precipitation is more complicated. Because of the well-known relationship between sensible heat flux and entrainment (Betts et al., 1996; Stull, 1988), H is well correlated to PBL depth (Figs. 6b and d respectively). The growth of the PBL throughout the day and the entrainment of dry free-tropospheric air are both dependent on the surface sensible heat flux (Pielke, 2001; Santanello et al., 2007). Also, partitioning of surface fluxes shows the Bowen ratio (H/LE) decreases with increasing soil moisture conditions consistent with decreasing (increasing) H (LE) flux with increasing soil moisture respectively (not shown).

Latent heat flux (Fig. 6a) is not strongly correlated with MSE (Fig. 6c) or surface humidity (Fig. 6f). This behavior can be at least partially explained by the reduced gradient between surface and 2-m when q_v is large, resulting in decreased LE. For this reason, MSE and q_v can be thought of as lagging, or being out of phase, with

LE. Differences in MSE are largely determined by surface humidity rather than 2-m potential temperature (Fig. 6e).

3.5 Evidence of mixing diagram limit bounds

Mixing diagrams (Betts, 1992; Santanello et al., 2011) are one way of viewing the thermodynamics of multi-day land–atmosphere interactions (Fig. 8). From Fig. 8, it is noticeable that there may be limit bounds within the mixing diagrams. Figure 7 shows these limits of PBL thermodynamic properties within energy space. The limit (bound) equations are:

$$c_p T = \begin{bmatrix} 30 \\ -0.4481 \\ 0.5251 \end{bmatrix} l_v q + \begin{bmatrix} 109000 \\ 325180 \\ 277008 \end{bmatrix}$$

The bounds were drawn to include 99% of the total amount of points. The sharp upper-right boundary represents an energetic limit, as it is close to the constant MSE=340 kJ kg^{-1} contour and depicts the thermodynamic state prior to convective overturning. This bound represents the energy buildup of the PBL to a warmer and moister state that is present prior to convective events. The few points outside the right limit are mainly from simulations with very low soil moisture conditions (θ=0.084 m^3 m^{-3}) and VF=1. Simulations with larger values of CIN showed the energy maximum is only weakly dependent on cap strength, although we suspect a stronger inversion (even higher CIN) may increase this energetic boundary toward higher MSE values. The diffuse left most bound likely results from wide variations in precipitation timing and magnitude leading to large differences in post-convection temperature and moisture conditions. The simulations near the lower-right bound represent simulations with full vegetation and moist soil conditions (θ=0.22-0.36 m^3 m^{-3}). As vegetation cover decreases to VF=0.5, the simulations move away from the

lower bound. This lower limit lies along a line of constant relative humidity of ∼80% coinciding with the bottom limit of the bounded triangle; therefore, this line is likely a relative humidity maximum bound.

3.6 Mixing diagrams throughout the parameter space

Figure 8a-c shows late afternoon (1600 local time LT) values of 2-m temperature and humidity for different values of soil moisture, vegetation fraction, and large-scale vertical motion. We are showing nine combinations of the θ, VF, and w_{ls} parameter space. Note that the θ=0.18 in (a), VF=1 in (b), and w_{ls}=0 in (c) simulations in Fig. 8 are equivalent. Large stars indicate the mean 1600 LT thermodynamic state for each simulation, with bars indicating variability ($\pm 1\sigma$).

The simulations with soil moisture set to wilting point (θ=0.084 in Fig. 8a) and the simulations with no vegetation (VF=0 in Fig. 8b) are characterized by a warm, dry state. This behavior is associated with small latent heat flux, large sensible heat flux, and substantial entrainment of dry, free-tropospheric air into the PBL. The 50% field capacity and field capacity (red and green stars respectively in Fig. 8a) show similar behavior in energy space, both moister and cooler than the wilting point simulations. Despite the substantial amount of MSE variability over the 90-day simulations, the simulation-mean MSE values are very similar (i.e., the mean values all lie very close to the ∼330 kJ kg^{-1} MSE line). Increasing vegetation cover produces results that are cooler and moister (Fig. 8b). As in the suite of simulations varying soil moisture, here too the mean MSE is approximately the same in all the simulations. Unlike variations in soil moisture and vegetation cover, large-scale vertical motion forcing has very little effect on the evolution of afternoon 2-m temperature and humidity in energy space (Fig. 8c). We note that the behavior in thermodynamic phase space (Fig. 8), which

is calculated using values at 1600 LT, differs from the statistics calculated over the entire day (Fig. 6).

Figure 8a, b show that fluxes of heat and moisture (governed by soil moisture and vegetation fraction) exert a greater influence on late-afternoon PBL thermodynamic properties than does large-scale vertical motion. Although the mean MSE values are remarkably similar across all the simulations in Fig. 8, the evolution of MSE during individual simulations likely projects onto CAPE and CIN, affecting convective precipitation characteristics. The boxed regions in Fig. 8 will be discussed next in order to evaluate the day-to-day coevolution of temperature and moisture in energy space.

3.7 20-day mixing diagram

Figure 9 shows the day-to-day evolution throughout thermodynamic space of a 20-day period (days 60–80) of the simulations in Fig. 8 corresponding to the subset of simulations with VF=1, θ=0.18 m^3m^{-3}, and w_{ls}=0 cm s^{-1}. This 20 day period is the "boxed" portion of Figure 8a-c.

The twenty days in Fig. 9 show the limit cycle of PBL properties in thermodynamic space at 1600 LT. Day 60 is followed by several days with no precipitation, and then a small convective event on day 65. This event was in the afternoon to evening hours of day 65 (Fig. 10a,b). This convective event is associated with a sharp decrease in 2-m temperature and humidity as the convection removes moisture and cools the PBL, leaving temperature and moisture substantially lower than on the day of the event. The 2-m temperature and moisture increase over the course of the next two days (Fig. 10a,b), followed by a precipitation event, which occurs during the late evening of day 67 and early morning hours on day 68.

Figure 9 shows an increase in temperature from day 67 to 68, but this can be

explained through Fig. 10a,b. The 1600 LT c_pT and ql_v values on days 67 and 68 are higher than expected, as the PBL should dry and cool following a precipitation event. Since the precipitation event was overnight, the 2-m temperature and humidity were allowed to recover after the event allowing the 1600 LT values to show an increase from the previous day. Even so, the temperature (Fig. 10a) shows a sharp decrease during the precipitation event.

3.8 Relationship between precipitation and PBL properties

Figure 11a-d shows the dependence of precipitation event magnitude on LE, H, PBL height, and MSE for simulations with full vegetation. Precipitation is weakly correlated with LE, with larger flux generally corresponding to greater precipitation magnitude (Fig. 11a). Similarly, precipitation and sensible heat flux H are negatively correlated (Fig. 11b). Low PBL heights (themselves associated with large values of LE and small values of H) accompany the strong precipitation events. Not surprisingly, Fig. 11b and c are very similar due to the strong control sensible heat flux has on PBL evolution. Relationships between both latent heat, sensible heat, and PBL height show two distinct clusters of behavior. Precipitation magnitude increases with MSE but does not exhibit the clustering behavior of the other quantities.

Figure 12a-d respectively show the relationship of precipitation event frequency on LE, H, PBL height, and MSE for the full-vegetation simulations. Precipitation event frequency is positively correlated with latent heat flux meaning that larger LE corresponds to more frequent precipitation events. This relationship is slightly more robust than the relationship between precipitation magnitude and latent heat flux (Fig. 12a).

Precipitation event frequency is negatively correlated with both sensible heat flux and PBL height (Fig. 12b and c). Smaller values of sensible heat flux and lower PBL

heights are generally associated with more frequent precipitation events, though there is a wide range of event frequency at lower values of these variables. Surface-based MSE and convective event frequency have a slight negative correlation. More frequent events are associated with lower MSE values, although a clustering of points around frequency values of 0.1 and 0.4 day^{-1} may be present.

3.9 What affects total precipitation?

Figure 13 shows total precipitation and its relationship with precipitation event magnitude and frequency. Similar to Porporato et al. (2003) who used observational data from the Kalahari transect in Africa, our study shows total 3-month summer precipitation is strongly correlated to event frequency rather than event magnitude (Fig. 13) indicating seasonal rainfall amounts are sensitive to rate of storm arrival rather than the event intensity itself. These results have strong implications for agricultural regions as precipitation behavior affects plant stress and productivity, and soil moisture stress can strongly influence growing season length (Seneviratne et al., 2010). Nippert et al. (2006) found that productivity of plants in the Konza Prairie (northeast Kansas) is significantly positively correlated with seasonal precipitation total, but changes in precipitation variability (magnitude and frequency) strongly influence plant health (i.e. plant water stress, soil moisture variability; Knapp et al., 2002; Nippert et al., 2006). Therefore, agricultural productivity within a changing climate will be affected by changes in not only precipitation total, but event frequency and intensity.

3.10 Sensitivity of convective precipitation to temperature nudging timescale

The nudging term, (τ_a), applied in the model acts as a simple representation of horizontal advection. Omitting nudging is equivalent to an infinite nudging timescale (not

shown) and in these simulations, drifts to a radiative-convective equilibrium solution that is too warm for the midlatitudes. Figure 14 shows how total precipitation, event frequency, and event magnitude vary with the nudging timescale, noting that all previously discussed simulations employed a nudging timescale of 3 days. Total precipitation (Fig. 14a-d) show an overall decrease as the nudging timescale increases. The 1-day temperature nudging suite, which represents completely "resetting" the temperature profile each day to its initial value, in particular shows substantially larger total precipitation values than the simulations with longer nudging timescales. For soil moisture values above θ=0.12 m^3 m^{-3}, all nudging timescale simulations exhibit various degrees of sensitivity to large-scale vertical motion. Precipitation events become less frequent with longer temperature nudging timescales (Fig. 14e-h), although precipitation remains infrequent under large-scale subsidence for all τ_a. Precipitation event magnitude is similar for all nudging timescales (Fig. 14i-l), with no obvious trend in magnitude with changing timescale.

3.11 Sensitivity to thermodynamic profile

We performed simulations varying the inversion magnitude and mid-tropospheric stability in order to assess sensitivity to an assumed thermodynamic profile. Simulations were performed with varying cap strength (control cap strengthened/weakened by +/- 2 K at its peak) to assess the effects of an inversion on convective precipitation properties (Segal et al., 1995). Total precipitation is only weakly dependent on inversion strength (Fig. 15a–c). All three capping inversion simulations showed similar total precipitation behavior, with a slight increase in total precipitation as the magnitude of the inversion is increased.

Similarly, precipitation event frequency (Fig. 15d–f) is only weakly dependent on inversion strength. Increasing the inversion strength decreases per-event precipita-

tion in the ascent regime, but precipitation event magnitude increases by ∼10 mm with decreasing inversion strength under regimes of strong subsidence (Fig. 15g–i). However, due to the small number of these stronger events, this has little impact on the total precipitation, but the more frequent, smaller events lead to larger values of total precipitation.

Differences in profile stability produces substantial differences in total precipitation (Fig. 16a–c). Stability was modified by varying potential temperature at and above 500 mb by 3 K. The more unstable sounding increases total precipitation over a large portion of the parameter space (Fig. 16a). Precipitation event frequency (Fig. 16d–f) shows the same general behavior with all three thermodynamic profiles, except in regimes of forced ascent as events here are less frequent as stability increases. Precipitation event magnitude is greatest for the control sounding, with the two other profiles leading to modest differences.

Chapter 4

Discussion and conclusions

We performed a series of simulations using a single-column configuration of WRF to explore influences on the character of convective precipitation. In particular, we explored regions of the parameter space of soil moisture, large-scale vertical motion, vegetation cover, advective (nudging) timescale, inversion strength, and mid-tropospheric stability. One goal of this study was to isolate key processes and determine how the PBL responds to surface conditions, which ultimately will affect deep convection. Our methodology is an extension of the approach of Clark and Arritt (1995), who utilized an SCM run for a short period of time (12 hours) with varying soil moistures and vegetation coverage to evaluate the effects of soil moisture on convective precipitation in the Great Plains. Our results explore the multi-day interactions of surface, boundary layer, free troposphere, and convective precipitation processes.

This WRF–SCM methodology bridges the gap between low-order bulk modeling approaches that predominantly concentrate on the influence of soil moisture and temperature on boundary-layer properties and convective triggering (Juang et al., 2007a; Siqueira et al., 2009), and longer-term 3D simulations (Jones and Brunsell, 2009a,b). Full 3D simulations that resolve deep convective processes are more physically realistic but are computationally expensive, enabling only small regions of parameter space to be explored. Our middle-of-the-road SCM approach employs a deep convec-

tive parameterization but also allows for a detailed exploration of parameter space. Running over a 90-day (or longer) period allows the model to represent the multi-day "memory" of the PBL and free troposphere not captured in single-day simulations.

The WRF–SCM approach captures both well-understood aspects of the sensitivity of deep convective precipitation characteristics to land-atmosphere system inputs (e.g. soil moisture) and possible unknown responses to other inputs (e.g. large-scale vertical motion, advective timescale). Our most notable findings are as follows:

- Simple, idealized SCM produces realistic precipitation characteristics, especially precipitation event magnitude, as estimated by the overlap of simulation and observational distributions. The simulations underestimated the mode of the intermittency and overestimated the right-hand tail of the distribution, leading to a much broader distribution of total precipitation than observed.

- As vegetation cover increases, soil moisture conditions become less influential in long-term precipitation behavior and characteristics.

- Total precipitation is determined largely by precipitation event frequency rather than magnitude. This is true for all vegetation fractions and throughout the whole θ–w_{ls} parameter space.

- MSE is not, by itself, a good predictor of the occurrence or magnitude of deep convective precipitation. Average MSE values may be similar across simulations, but the resulting precipitation characteristics may be substantially different.

- Precipitation characteristics are strongly sensitive to large-scale vertical motion, but predominantly in subsidence regimes. Precipitation event magnitude is enhanced in subsidence regimes, but events are less frequent. Total precipitation

is maximized, however, with forced ascent due to more frequent but less intense events. This dependence on w_{ls} is robust across different thermodynamic profiles and advective timescales. However, this dependence on w_{ls} does not hold for bare soil.

- Total precipitation decreases substantially as the nudging timescale, τ_a, is increased. Precipitation event magnitude is comparable across nudging timescales, but intermittency varies in the forced ascent regime as events become less frequent as nudging timescale is increased. Event frequency, however, is comparable across nudging timescales in the subsidence regime.

- Altering inversion strength slightly impacts total precipitation and event frequency. Event magnitude is maximized in the subsidence regime for all cap strengths, with the strongest inversion associated with weaker event precipitation. Total precipitation is strongly dependent upon free-tropospheric stability, with greater precipitation totals seen with the more unstable profile; however, event frequency is roughly consistent across all three values of stability, except in the forced vertical ascent regime.

We wish to point out a few caveats present in such a highly idealized numerical simulation approach, above and beyond that of the simple SCM framework with parameterized deep convective processes. We maintain a constant soil moisture value in order to explore the sensitivity of PBL and precipitation processes to that specific soil moisture value. This sacrifices the interactive nature of soil moisture in order to be more statistically confident in the simulation outcomes (though in most cases we have not formally evaluated statistical significance). When assuming constant soil moisture, the only interactive component of our simulations is the feedback between PBL processes and deep convection. The feedback between soil moisture and

convective precipitation is important (Eltahir, 1998; Findell and Eltahir, 2003; Jones and Brunsell, 2009a), but our study focuses on the one-way sensitivity of convective precipitation on surface and atmospheric properties.

We employ nudging of the temperature profile back to its initial state as a proxy for large-scale advective tendencies and test the sensitivity of the model to differences in this nudging timescale. We also impose large-scale vertical motion that is constant over the course of the simulation. It is obvious that large-scale advection and vertical motion are coupled, a coupling which our approach ignores. The reasonable behavior of our results suggest that this synoptic coupling impacts the day-to-day variability of the simulation less than the drying and warming of the SCM by deep convective processes. Future simulations could impose synoptic variability in a much more systematic fashion.

The simulations produce the well-understood relationship between soil moisture and surface latent and sensible heat fluxes, with greater values of soil moisture associated with increased latent heat flux. Total precipitation generally increases with increasing soil moisture, consistent with the regional climate simulations of Jones and Brunsell (2009a,b). The decreasing influence of soil moisture as vegetation cover is increased is consistent with the one-day simulations of Clark and Arritt (1995). In the bare soil conditions, total precipitation increases more or less linearly with soil moisture, whereas when vegetation is present the increase in precipitation occurs much more abruptly and at low values of soil moisture.

Unsurprisingly, the choice of thermodynamic profile affects convective precipitation. Changing the stability of the inversion only modestly affects total precipitation, and preserves the precipitation behavior in θ–w_{ls} space. Over most of the θ–w_{ls} parameter space, event frequency varies only weakly, which we interpret as the inversion not being the ultimate determining factor on whether convection is triggered on any

given day. In weakly forced situations (w_{ls}=0), increasing inversion stability actually results in a slight enhancement of event precipitation. This behavior is likely due to instability accumulating in the boundary layer prior to the eroding of the inversion and was also noted in the simulations of Clark and Arritt (1995). However, increasing inversion strength suppresses event magnitude when there is forced subsidence. Increasing the mid-tropospheric lapse rate results in an increase in total precipitation via increasing the event frequency when there is forced upward vertical motion; event magnitude changes are minimal except for strongly subsident regimes.

Jones and Brunsell (2009b) found that for constant vegetation conditions, increasing soil moisture resulted in more frequent precipitation events. Our study shows event frequency is greatly amplified with increasing soil moisture conditions in the bare soil case, but shows less of a dependence on soil moisture as vegetation cover increases. Even so, our study is consistent with Dai (2001) who found observed summertime convection occurs 10-30% of the time during the summertime months. This holds true in our simulations, especially in the slight subsidence and weakly forced regimes when vegetation is present and when 0.15 m^3 m^{-3} $< \theta <$0.3 m^3 m^{-3} in the bare soil simulations. Stephens et al. (2010) suggest models produce more frequent, weak events which Dai and Trenberth (2004) and Sun et al. (2006) attribute to rapid firing of convection without CIN (large-scale subsidence) allowing instability (CAPE) to build up prior to a convective event. We see these low magnitude, high frequency events in the strong vertical ascent regimes, but less so in neutral ascent and subsidence regimes where instability (CAPE) is encouraged to build prior to a convective event.

The advantage of this SCM approach is that it encourages the exploration of wide range of parameter space(s) at relatively low computational expense. Because much is still unknown about feedbacks between soil moisture and precipitation, future

simulations using this SCM framework should allow soil moisture to vary interactively.

Table 1 Model simulations performed; θ–soil moisture, w_{ls}– large-scale vertical motion, VF–vegetation fraction, τ_n–temperature nudging timescale.

θ (m^3 m^{-3})	w_{ls} (cm s^{-1})	VF	τ_n (days)	Cap strength (K)	$>$ 500 mb pot. temp. (K)
0.36	-0.5	1	1	+ 2	+ 3
0.32	-0.3	0.5	3	control	control
0.27	-0.1	0	5	− 2	− 3
0.22	0		7		
0.18	0.1				
0.12	0.3				
0.084	0.5				

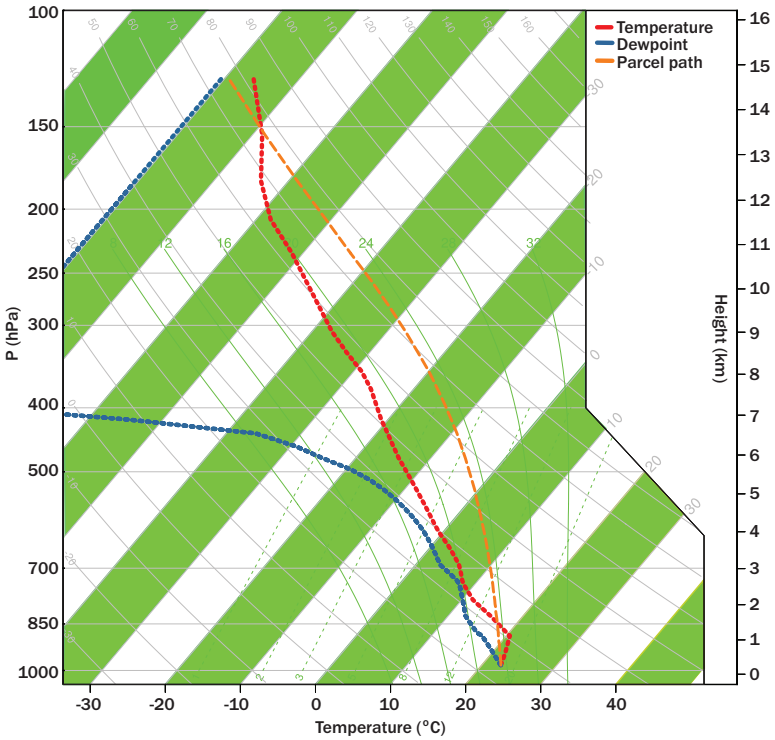

Fig. 1 Initial skew-t sounding used for all control simulations based on observations from Topeka, KS; temperature (red), dew point (blue) and lifted parcel path (orange) shown.

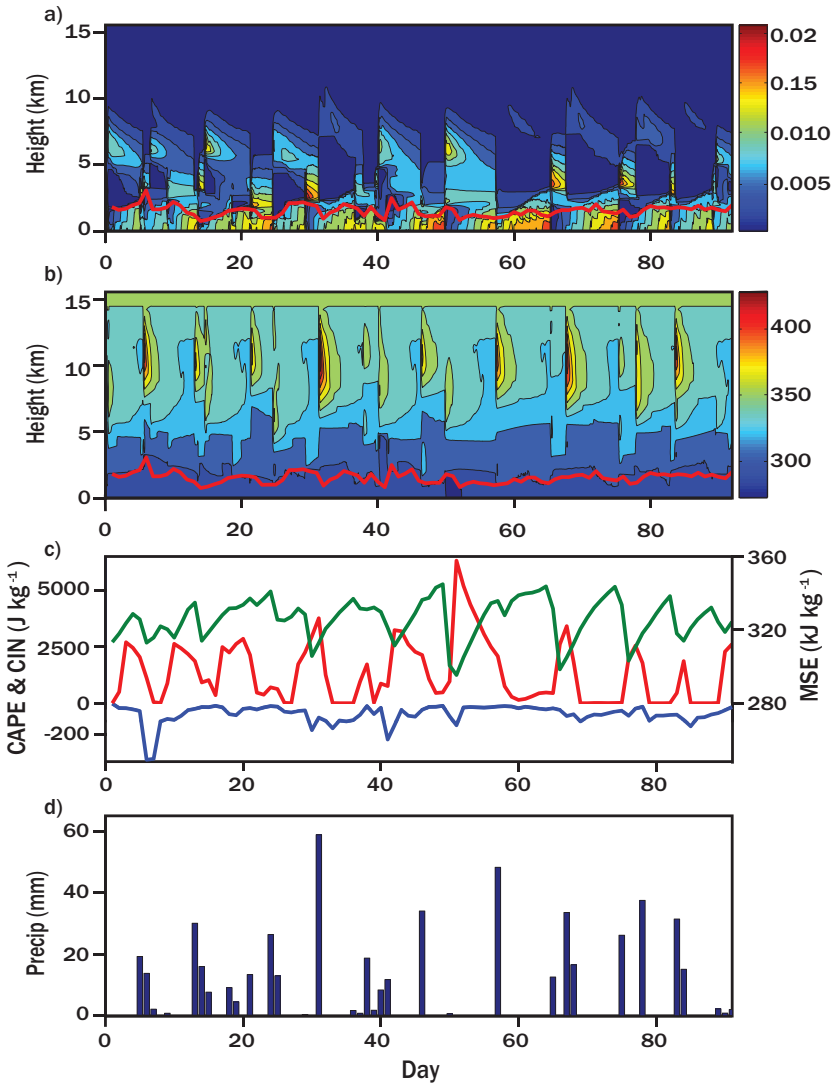

Fig. 2 Simulation results for vegetation cover=100%, θ=0.18 m^3 m^{-3}, w_{ls}=0 cm s^{-1} (control run). (a) Mixing ratio (kg kg^{-1}) evolution, PBL height (red line); (b) Potential temperature evolution (K), PBL height (red line); (c) Daily average CAPE (J kg^{-1}; red), CIN (J kg^{-1}; blue), and MSE (kJ kg^{-1}; green); (d) Daily precipitation total (mm)

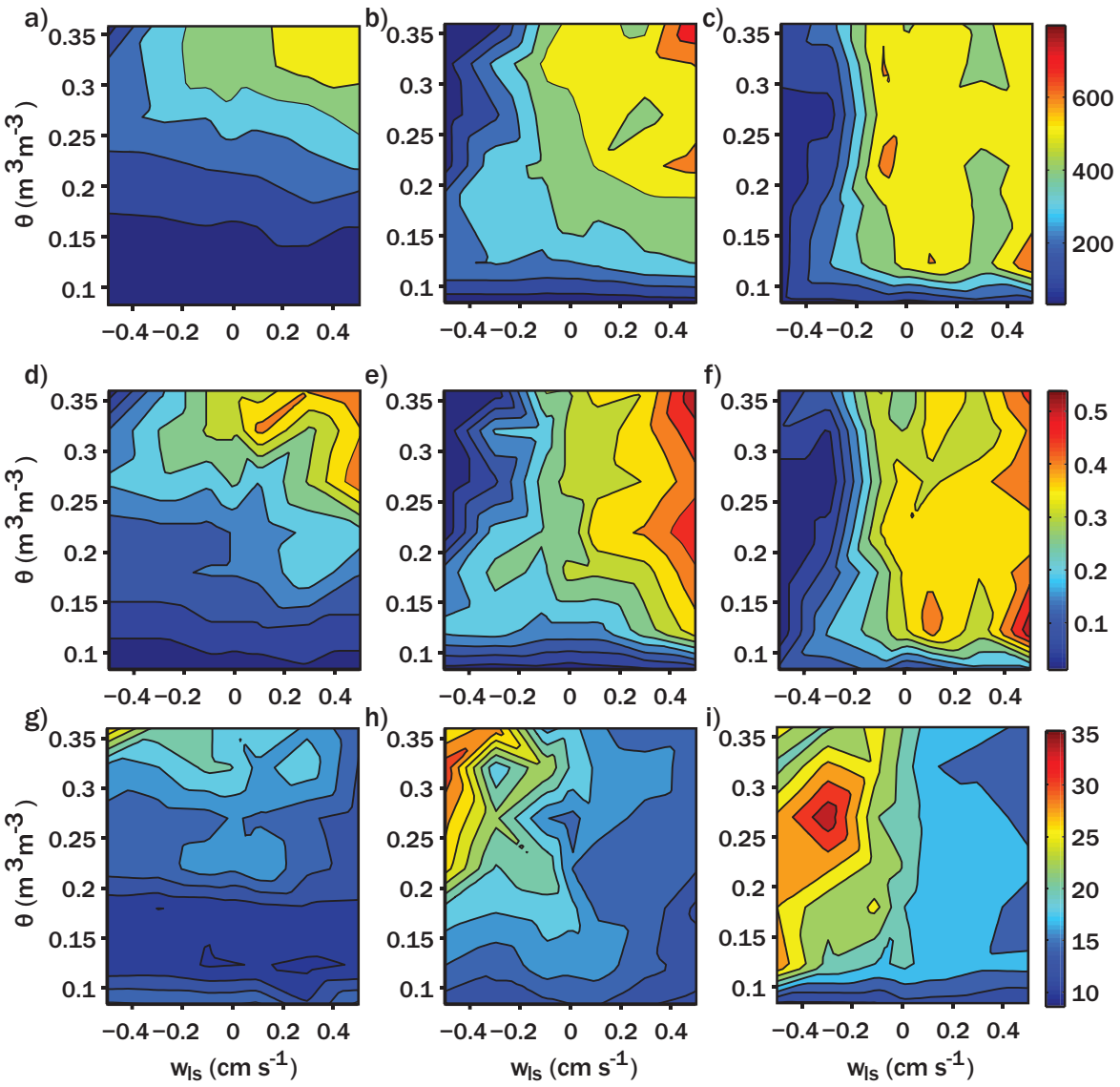

Fig. 3 Precipitation behavior throughout the soil moisture (θ) – large-scale vertical motion (w_{ls}) parameter space. (a-c) Total precipitation (mm), (d-f) Precipitation frequency (day^{-1}), (g-i) Precipitation magnitude (mm). Columns left to right represent 0, 50, and 100% vegetation cover respectively.

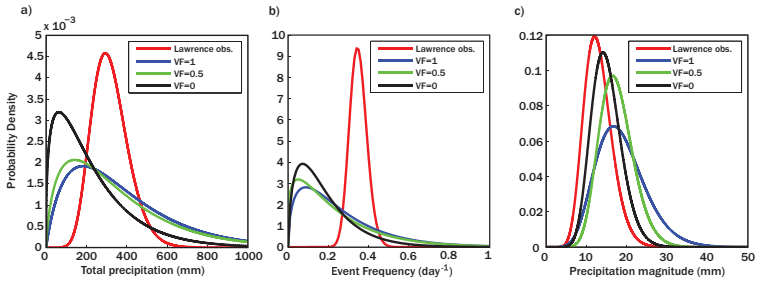

Fig. 4 Precipitation PDF's for a) Total precipitation (mm), b) Precipitation event frequency (day^{-1}), c) Precipitation magnitude (mm). Red lines represent PDF's for Lawrence, KS observations, blue lines represent PDF's for all VF=1 simulations, green lines represent PDF's for all VF=0.5 simulations, and black lines represent PDF's for all bare soil simulations.

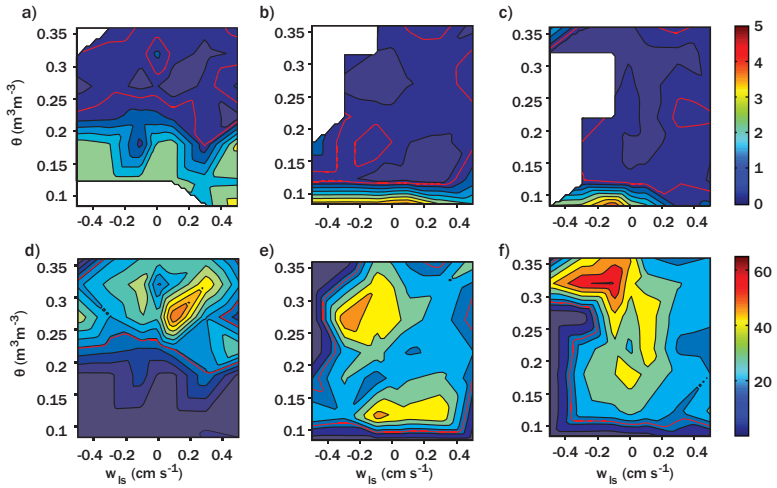

Fig. 5 Shape (α; top row) and scale (β; bottom row) parameter of precipitation event magnitude (mm) for a,d) VF=0, b,e) VF=0.5, and c,f) VF=1 simulations. Red overlay lines are alpha and beta contours for Lawrence, KS observational data. Blank sections indicate areas of the parameter space that have too few events to estimate parameters.

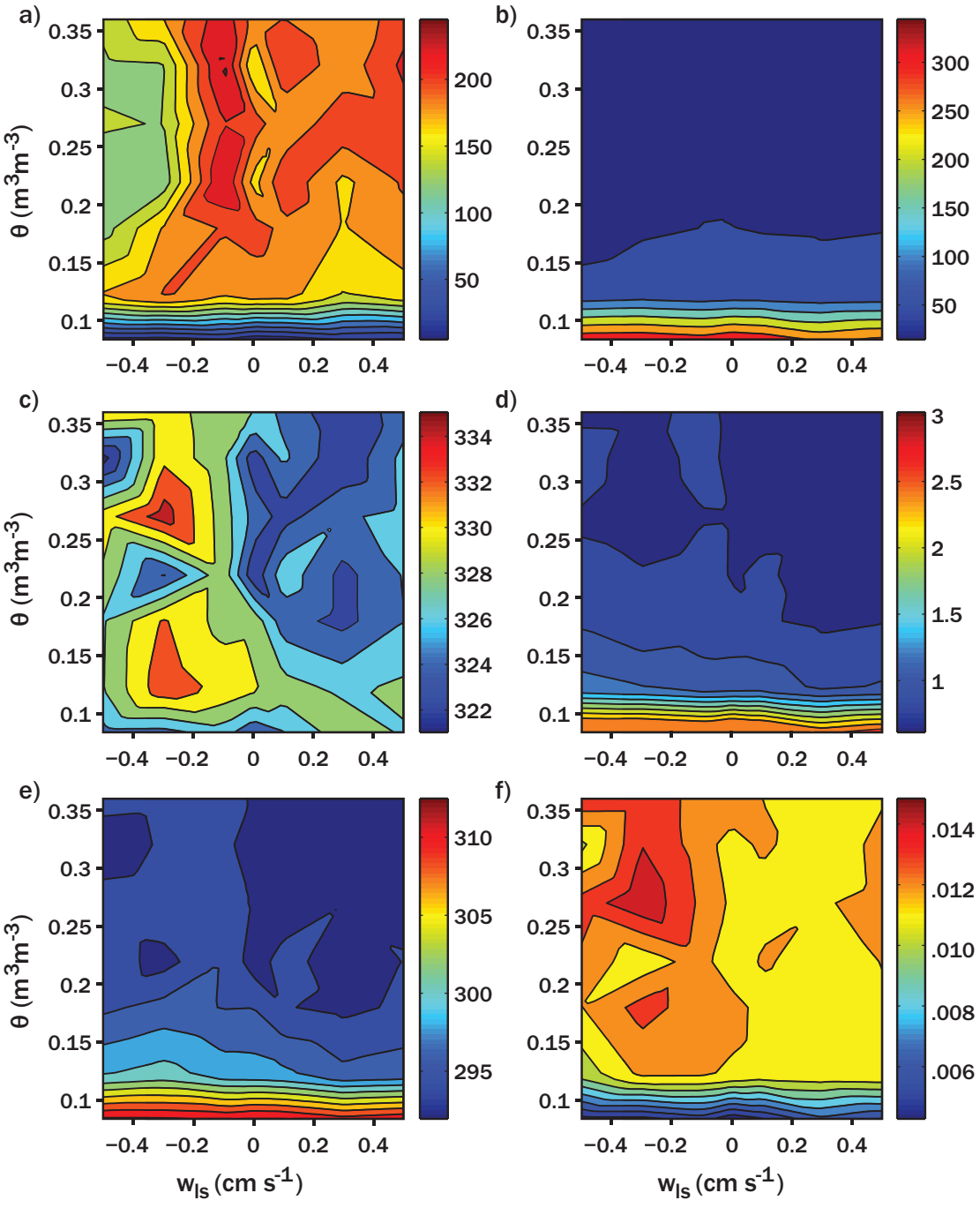

Fig. 6 Average daytime (12Z - 20Z) (a) latent heat flux (W m^2) (b) sensible heat flux (W m^2). (c) MSE (kJ kg^{-1}), (d) PBL height (km), (e) 2-m potential temperature (K), (f) 2-m mixing ratio (kg kg^{-1})

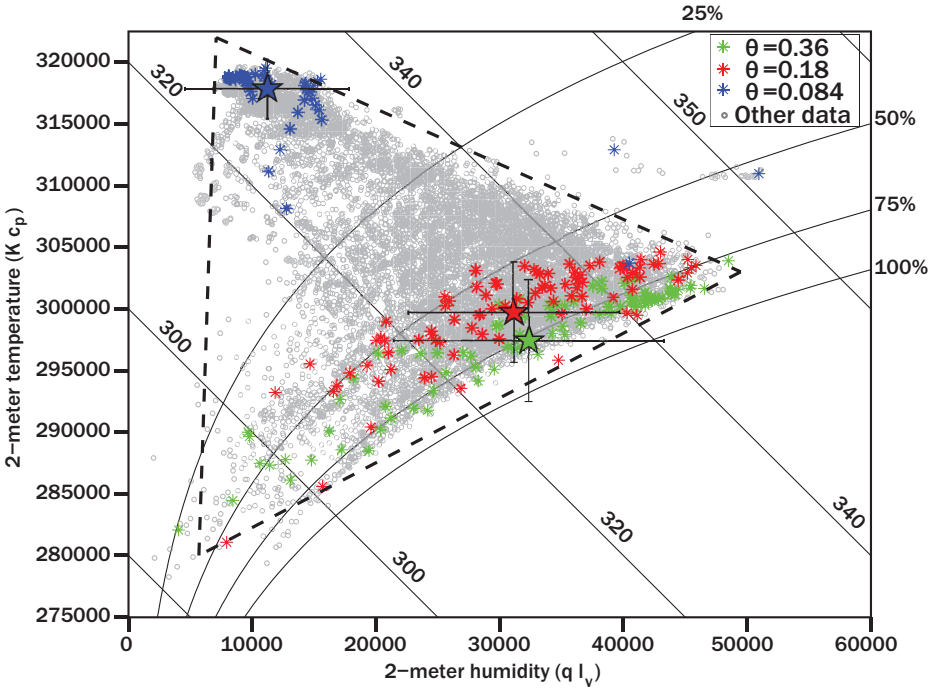

Fig. 7 Mixing diagram for all simulations. Simulations with soil moisture set to field capacity (green), 50% field capacity (red), and wiling point (blue) with w_{ls}=0 cm s^{-1}, 100% vegetation cover highlighted. Each point on this figure taken at 1600 LT, and every simulation with 3-day nudging to the sounding is included. Overlaid are lines of constant MSE (kJ kg^{-1}) and lines of constant relative humidity (RH; %)

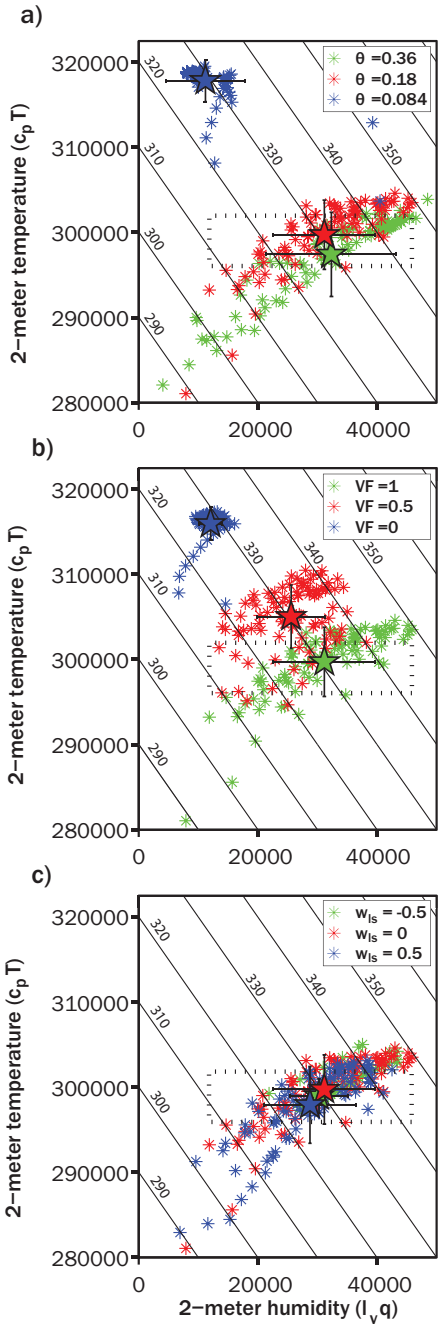

Fig. 8 Mixing diagram for (a) Field capacity (green), 50% field capacity (red), and wiling point (blue) with w_{ls}=0 cm s^{-1}, 100% vegetation cover; (b) 100% veg. cover (green), 50% veg. cover (red), and 0% veg. cover (blue) with w_{ls}=0 cm s^{-1}, θ=0.18 m^3 m^{-3}; (c) Subsidence (green), no vertical forcing (red), and upward vertical forcing (blue) with 100% vegetation cover, θ=0.18 m^3 m^{-3}. Overlaid are lines of constant MSE (kJ kg^{-1}).

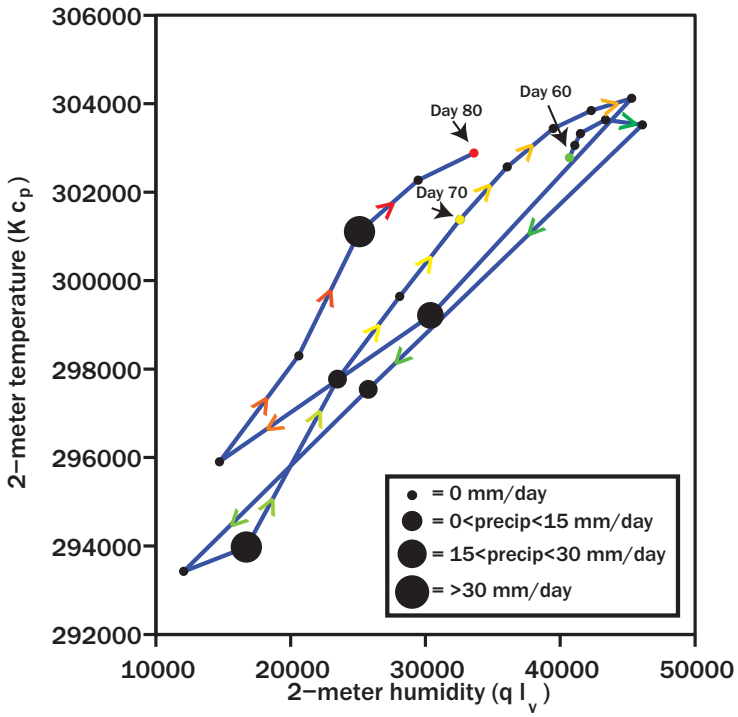

Fig. 9 Mixing diagram for 20-day (days 60-80) period from "boxed region" in Fig. 8 representing the control simulation. The 'start day' (day 60) is represented by the green dot, the 'middle day' (day 70) is the yellow dot, and the 'end day' is the red dot. There were a total of four precipitation events over this 20-day period (one event spanning 2 days), and the magnitude of these events are represented by the size of the dot for a given day. The smallest dots represent days when there was no precipitation.

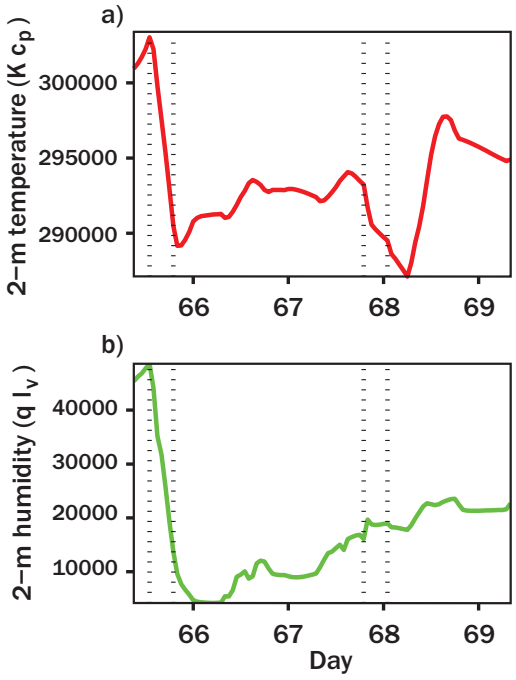

Fig. 10 (a) 2-m temperature, and (b) 2-m humidity for days 65-69 of Fig. 9. Dashed lines indicate timing of precipitation events.

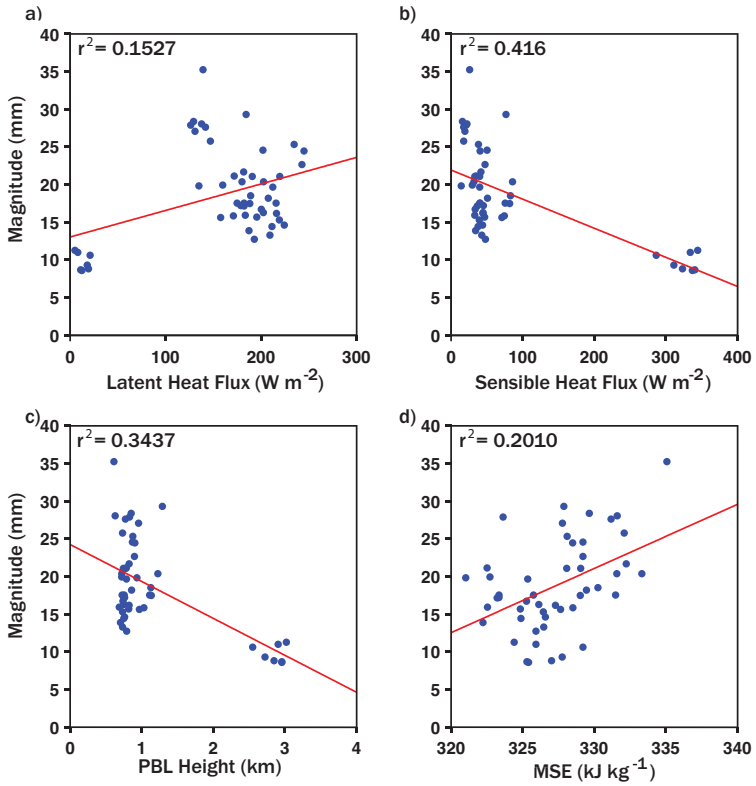

Fig. 11 Precipitation magnitude (mm) and its relationship with daytime mean (12Z - 20Z) (a) latent heat flux (W m^{-2}), (b) sensible heat flux (W m^{-2}), (c) PBL height (km), and (d) MSE (kJ kg^{-1}). All for 100% vegetation cover parameter space simulations.

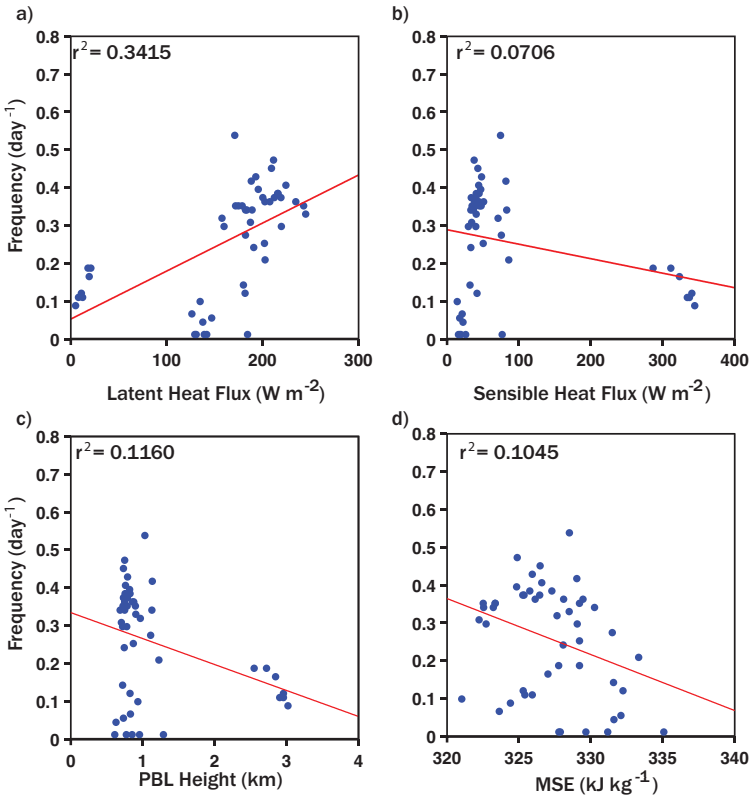

Fig. 12 Precipitation event frequency (day^{-1}) and its relationship with daytime mean (12Z - 20Z) (a) latent heat flux (W m^{-2}), (b) sensible heat flux (W m^{-2}), (c) PBL height (km), and (d) MSE (kJ kg^{-1}). All for 100% vegetation cover parameter space simulations.

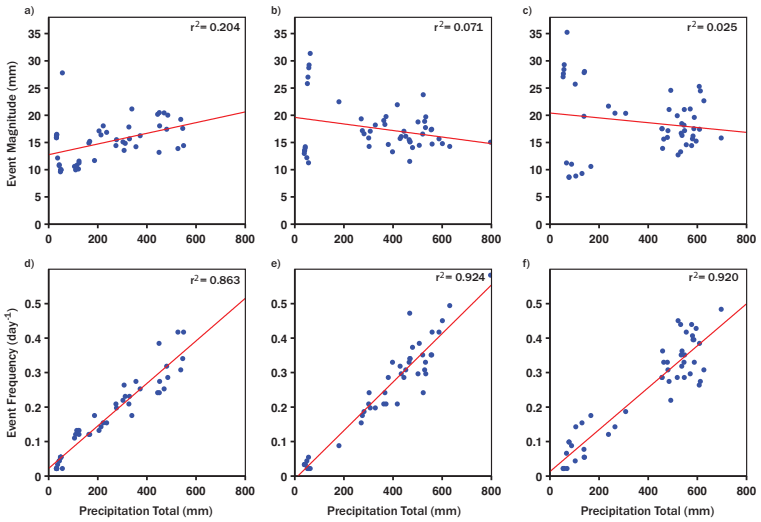

Fig. 13 (a-c) Precipitation total vs. precipitation event magnitude (mm) for VF=0, 0.5, 1 respectively, (d-f) Precipitation total vs. precipitation event frequency (day^{-1}) for VF=0, 0.5, 1 respectively

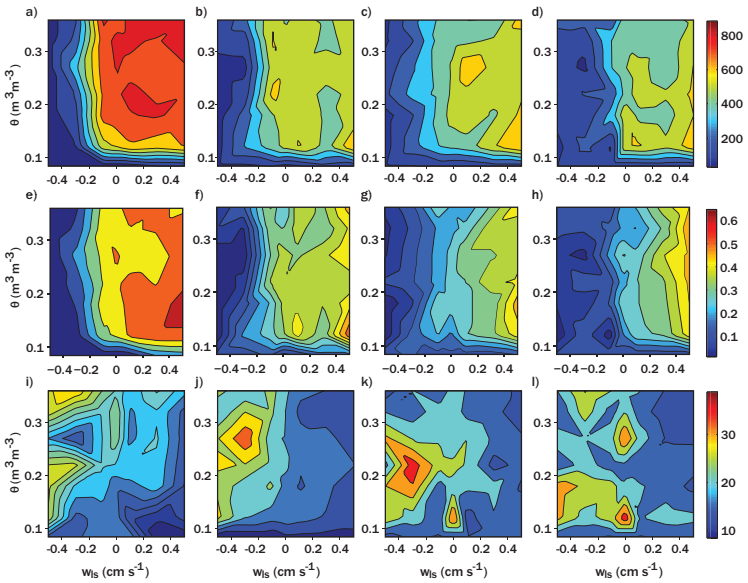

Fig. 14 Precipitation behavior of (a-d) Total precipitation (mm); (e-h) Precipitation event frequency (day^{-1}); (i-l) Precipitation event magnitude (mm). All figures are valid for VF=1 simulations. Columns from left to right represent 1-day, 3-day (control), 5-day, and 7-day temperature nudging respectively.

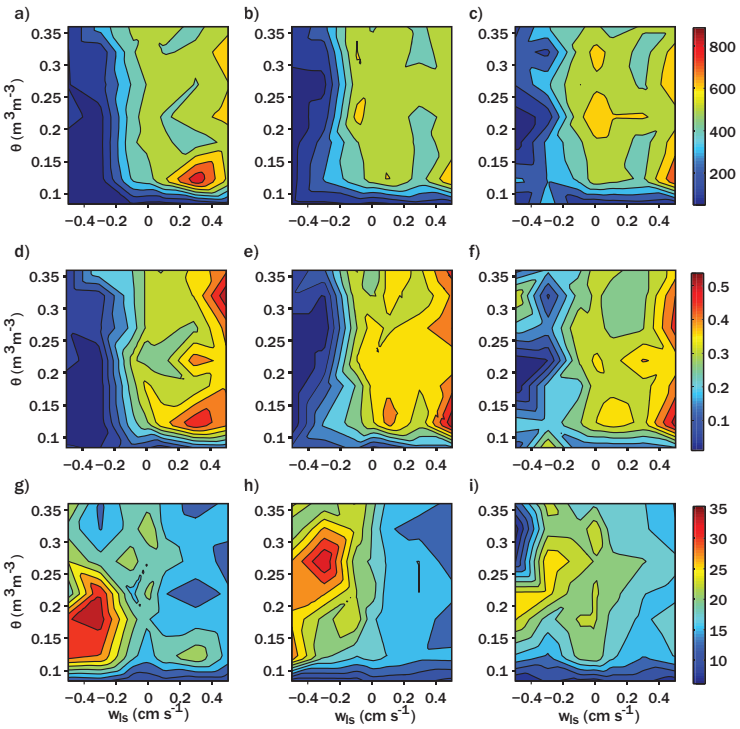

Fig. 15 Precipitation behavior for (a-c) Total precipitation (mm); (e-h) Precipitation event frequency (day^{-1}); (i-l) Precipitation event magnitude (mm). All figures are valid for VF=1 simulations. Columns left to right represent small capping inversion, moderate cap (control), and strong cap respectively.

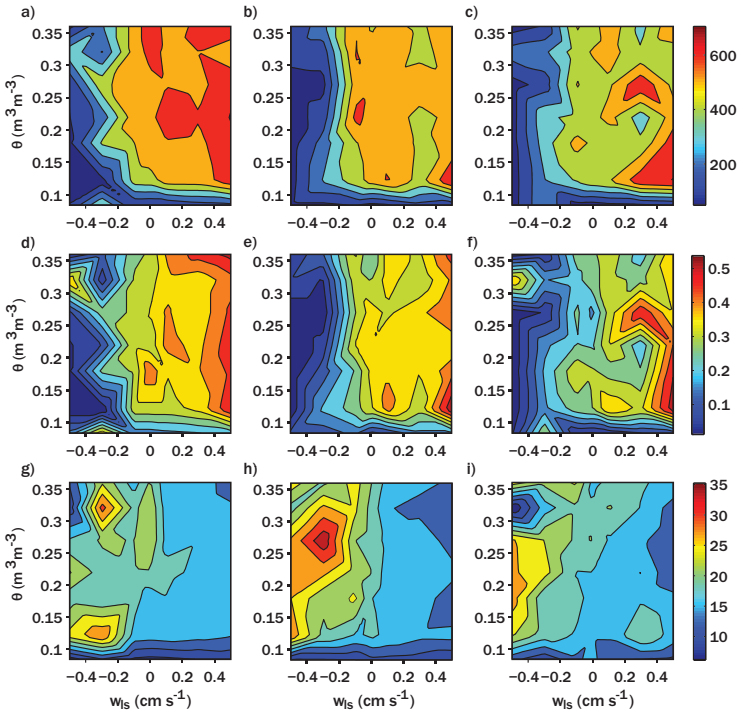

Fig. 16 Precipitation behavior for VF=1 of (a-c) Total precipitation (mm); (d-f) Precipitation event frequency (day^{-1}); (g-i) Precipitation event magnitude (mm). Columns left to right represent the more unstable, control, and more stable upper air simulations respectively.

Bibliography

Betts, A., 1992: Fife atmospheric boundary layer budget methods. *J. Geophys. Res.*, **97D**, 18 523–18 531.

Betts, A. K., 2000: Idealized model for equilibrium boundary layer over land. *J. Hydrometeor.*, **1 (6)**, 507–523.

Betts, A. K., J. H. Ball, A. C. M. Beljaars, M. Miller, and P. A. Viterbo, 1994: Coupling between land-surface, boundary-layer parameterizations and rainfall on local and regional scales: lessons from the wet summer of 1993. Conference on Global Change Studies: Amer. Meteor. Society Proceedings 74th Annual Meeting, Nashville, TN, Jan. 23-28, 174–181.

Betts, A. K., J. H. Ball, A. C. M. Beljaars, M. J. Miller, and P. A. Viterbo, 1996: The land surface-atmosphere interaction: A review based on observational and global modeling perspectives. *J. Geophys. Res.*, **101**, 7209–7225.

Brunsell, N. A., 2006: Characterization of land-surface precipitation feedback regimes with remote sensing. *Remote Sens. Environ.*, **100 (2)**, 200–211.

Chen, F. and J. Dudhia, 2001: Coupling an advanced land surface-hydrology model with the Penn State-NCAR MM5 modeling system. Part I: Model implementation and sensitivity. *Mon. Wea. Rev.*, **129 (4)**, 569–585.

Clark, C. A. and P. W. Arritt, 1995: Numerical simulations of the effect of soil moisture and vegetation cover on the development of deep convection. *J. Appl. Meteor.*, **34 (9)**, 2029–2045.

Dai, A., 2001: Global precipitation and thunderstorm frequencies. Part I: Seasonal and interannual variations. *J. Climate*, **14 (6)**, 1092–1111.

Dai, A., 2006: Precipitation characteristics in eighteen coupled climate models. *J. Climate*, **19 (18)**, 4605–4630.

Dai, A. and K. E. Trenberth, 2004: The diurnal cycle and its depiction in the community climate system model. *J. Climate*, **17 (5)**, 930–951.

De Ridder, K., 1997: Land surface processes and the potential for convective precipitation. *J. Geophys. Res.*, **102 (D25)**, 30 085–30.

Dearden, C., 2009: Investigating the simulation of cloud microphysical processes in numerical models using a one-dimentional dynamical framework. *Atmos. Sci. Let.*, **10**, 207–214.

Dudhia, J., 1989: Numerical study of convection observed during the winter monsoon experiment using a mesoscale two-dimensional model. *J. Atmos. Sci.*, **46 (20)**, 3077–3107.

Eagleson, P. S., 1978: Climate, soil, and vegetation: 1. introduction to water balance dynamics. *Water Resources Research*, **14 (5)**, 705–712.

Ek, M., K. Mitchell, Y. Lin, E. Rogers, P. Grunmann, V. Koren, G. Gayno, and J. D. Tarpley, 2003: Implementation of Noah land surface model advances in the National Centers for Environmental Prediction operational mesoscale Eta model. *J. Geophys. Res*, **108 (D22)**, 8851.

Eltahir, E. A. B., 1998: A soil moisture-rainfall feedback mechanism 1. Theory and observations. *Water Resour. Res.*, **34 (4)**, 765–776.

Entekhabi, D., I. Rodriguez-Iturbe, and F. Castelli, 1996: Mutual interaction of soil moisture state and atmospheric processes. *Journal Hydrol.*, **184 (1)**, 3–17.

Findell, K. L. and E. A. B. Eltahir, 2003: Atmospheric controls on soil moisture-boundary layer interactions. Part I: Framework development. *J. Hydrometeor.*, **4 (3)**, 552–569.

Furrer, E. M. and R. W. Katz, 2008: Improving the simulation of extreme precipitation events by stochastic weather generators. *Water Resour. Res.*, **44 (12)**, W12 439.

Guichard, F., et al., 2004: Modeling the diurnal cycle of deep precipitating convection over land with cloud-resolving models and single-column models. *Q. J. Ro. Meteor. Soc.*, **130 (604)**, 3139–3172.

Hohenegger, C., P. Brockhaus, C. S. Bretherton, and C. Schär, 2009: The soil moisture-precipitation feedback in simulations with explicit and parameterized convection. *J. Climate*, **22 (19)**, 5003–5020.

Hong, S. Y., Y. Noh, and J. Dudhia, 2006: A new vertical diffusion package with an explicit treatment of entrainment processes. *Mon. Wea. Rev.*, **134 (9)**, 2318–2341.

Husak, G. J., J. Michaelsen, and C. Funk, 2006: Use of the gamma distribution to represent monthly rainfall in Africa for drought monitoring applications. *Int. J. Climatol.*, **27 (7)**, 935–944.

Janjic, Z. I., 1994: The step-mountain eta coordinate model: Further developments

of the convection, viscous sublayer, and turbulence closure schemes. *Mon. Wea. Rev.*, **122 (5)**, 927–945.

Jones, A. R. and N. A. Brunsell, 2009a: Energy balance partitioning and net radiation controls on soil moisture-precipitation feedbacks. *Earth Interact.*, **13 (2)**, 1–25.

Jones, A. R. and N. A. Brunsell, 2009b: A scaling analysis of soil moisture–precipitation interactions in a regional climate model. *Theor. Appl. Climatol.*, **98 (3)**, 221–235.

Juang, J., G. Katul, A. Porporato, P. Soty, M. Siqueira, M. Detto, H. Kim, and R. Oren, 2007a: Eco-hydrological controls on summertime convective rainfall triggers. *Glob. Change Biol.*, **13 (4)**, 887–896.

Juang, J., A. Porporato, P. Stoy, M. Siqueira, A. Oishi, M. Detto, H. S. Kim, and G. G. Katul, 2007b: Hydrologic and atmospheric controls on initiation of convective precipitation events. *Water Resour. Res.*, **43 (3)**, W03 421.

Knapp, A. K., et al., 2002: Rainfall variability, carbon cycling, and plant species diversity in a mesic grassland. *Science*, **298 (5601)**, 2202–2205.

Koster, R. D. and P. S. Eagleson, 1990: A one-dimensional interactive soil-atmosphere model for testing formulations of surface hydrology. *J. Climate*, **3 (6)**, 593–606.

Koster, R. D., et al., 2006: Glace: the global land-atmosphere coupling experiment. part i: overview. *Journal of Hydrometeorology*, **7 (4)**, 590–610.

Lin, Y. L., R. D. Farley, and H. D. Orville, 1983: Bulk parameterization of the snow field in a cloud model. *J. Clim. Appl. Meteorol.*, **22 (6)**, 1065–1092.

McPherson, R. A., 2007: A review of vegetation—atmosphere interactions and their influences on mesoscale phenomena. *Prog. Phys. Geog.*, **31 (3)**, 261–285.

Meene, M. J., C. N. Williams, and R. S. Vose, 2011: United States Historical Climatology Network Daily Temperature, Precipitation, and Snow Data. Tech. rep., Carbon Dioxide Information Analysis Center, Oak Ridge National Laboratory, Oak Ridge, Tennessee.

Mlawer, E. J., S. J. Taubman, P. D. Brown, M. J. Iacono, and S. A. Clough, 1997: Radiative transfer for inhomogeneous atmospheres: RRTM, a validated correlated-k model for the longwave. *J. Geophys. Res.*, **102 (D14)**, 16 663–16 682.

Nippert, J. B., A. K. Knapp, and J. M. Briggs, 2006: Intra-annual rainfall variability and grassland productivity: can the past predict the future? *Plant Ecology*, **184 (1)**, 65–74.

Pal, J. and E. Eltahir, 2001: Pathways relating soil moisture conditions to future summer rainfall within a model of the land-atmosphere system. *J. Climate*, **14 (6)**, 1227–1242.

Petrie, M. and N. Brunsell, 2012: The role of precipitation variability on the ecohydrology of grasslands. *Ecohydrology*, **5 (3)**, 337–345.

Pielke, R. A., 2001: Influence of the spatial distribution of vegetation and soils on the prediction of cumulus convective rainfall. *Rev. Geophys.*, **39 (2)**, 151–178.

Porporato, A., F. Laio, L. Ridolfi, K. K. Caylor, and I. Rodriguez-Iturbe, 2003: Soil moisture and plant stress dynamics along the kalahari precipitation gradient. *J. Geophys. Res.*, **108 (D3)**, 4127.

Rawls, W., D. Brakensiek, and K. Saxton, 1982: Estimation of soil water properties. *Trans. Asae*, **25 (5)**, 1316–1320.

Santanello, J. A., M. A. Friedl, and M. B. Ek, 2007: Convective planetary boundary layer interactions with the land surface at diurnal time scales: Diagnostics and feedbacks. *J. Hydrometeor.*, **8 (5)**, 1082–1097.

Santanello, J. A., C. D. Peters-Lidard, and S. V. Kumar, 2011: Diagnosing the sensitivity of local land-atmosphere coupling via the soil moisture-boundary layer interaction. *J. Hydrometeor.*, **12 (5)**, 766–786.

Schlemmer, L., C. Hohenegger, J. Schmidli, and C. Schär, 2012: Diurnal equilibrium convection and land surface–atmosphere interactions in an idealized cloud-resolving model. *Q. J. Roy. Meteor. Soc.*

Segal, M., R. W. Arritt, C. Clark, R. Rabin, and J. Brown, 1995: Scaling evaluation of the effect of surface characteristics on potential for deep convection over uniform terrain. *Mon. Wea. Rev.*, **123 (2)**, 383–400.

Seneviratne, S., T. Corti, E. Davin, M. Hirschi, E. Jaeger, I. Lehner, B. Orlowsky, and A. J. Teuling, 2010: Investigating soil moisture–climate interactions in a changing climate: A review. *Earth-Sci. Rev.*, **99 (3)**, 125–161.

Siqueira, M., G. Katul, and A. Porporato, 2009: Soil moisture feedbacks on convection triggers: the role of soil-plant hydrodynamics. *J. Hydrometeor.*, **10 (1)**, 96–112.

Skamarock, W. C., J. B. Klemp, J. Dudhia, D. O. Gill, D. M. Barker, W. Wang, and J. G. Powers, 2005: A description of the Advanced Research WRF Version 2. Tech. rep., DTIC Document.

Stein, U. and P. Alpert, 1993: Factor separation in numerical simulations. *J. Atmos. Sci.*, **50**, 2107–2115.

Stensrud, D. J., 2007: *Parameterization schemes: Keys to understanding numerical weather prediction models*. Cambridge University Press.

Stephens, G. L., et al., 2010: Dreary state of precipitation in global models. *J. Geophys. Res.*, **115 (D24)**, D24 211.

Stull, R. B., 1988: *An introduction to boundary layer meteorology*, Vol. 13. Springer.

Sun, Y., S. Solomon, A. Dai, and R. W. Portmann, 2006: How often does it rain? *J. Climate*, **19 (6)**, 916–934.

Trenberth, K. E., A. Dai, R. M. Rasmussen, and D. B. Parsons, 2003: The changing character of precipitation. *Bull. Amer. Meteor. Soc.*, **84 (9)**, 1205–1218.

Trier, S. B., F. Chen, and K. W. Manning, 2004: A study of convection initiation in a mesoscale model using high-resolution land surface initial conditions. *Mon. Wea. Rev.*, **132 (12)**, 2954–2976.

Trier, S. B., F. Chen, K. W. Manning, M. A. LeMone, and C. A. Davis, 2008: Sensitivity of the PBL and precipitation in 12-day simulations of warm-season convection using different land surface models and soil wetness conditions. *Mon. Wea. Rev.*, **136 (7)**, 2321–2343.